Electronic Supplementary Material (ESI) for Journal of Materials Chemistry A.
This journal is © The Royal Society of Chemistry 2021

Supplementary Information

P-doped SnFe nanocubes decorated with PdFe alloy nanoparticles for ethanol fuel cells

Dimpul Konwar†, Padmini Basumatary†, UnHo Lee, and Young Soo Yoon*

Department of Materials Science and Engineering, Gachon University, Bokjung-dong, Seongnam-si, Gyeonggi-Do, 1342, Republic of Korea

*Corresponding author. Y. S. Yoon
Tel. +82 10 8766 5558; Fax: +82 31 750 8988.
E-mail: benedicto@gachon.ac.kr
†Both authors contributed equally.

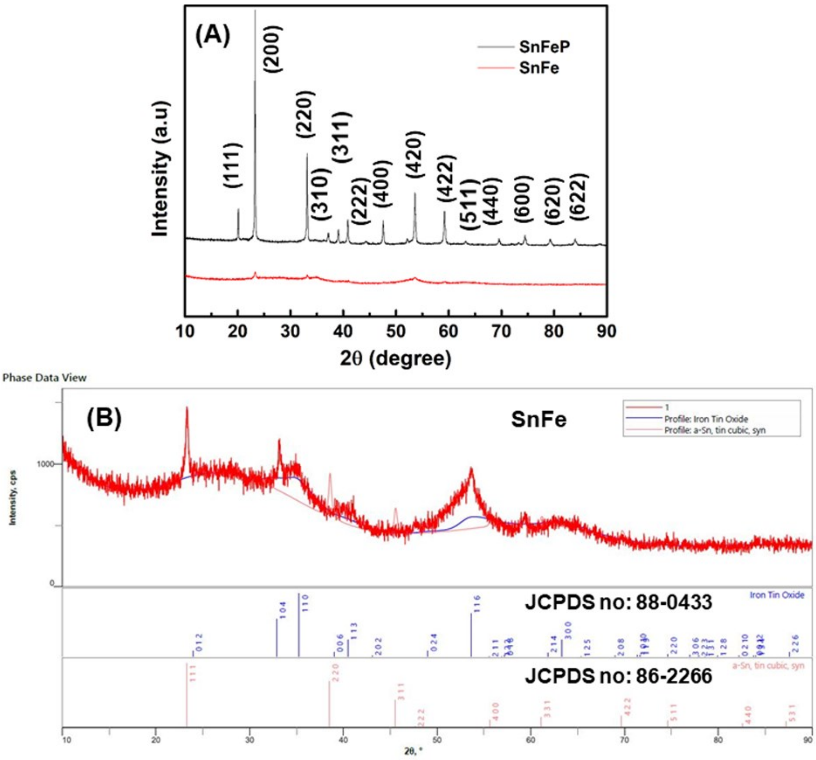

Fig. S1. XRD pattern of (A) SnFeP and SnFe. (B) Peak fitting of SnFe.

Table ST1. Particle sizes and crystallographic data of the as-prepared catalysts.

Catalysts	**2Θ (220) peak**	**2Θ (111) peak**	**Ɛ (nm)**	**D[c] (nm)**	**η[d]**	**η[d] (%)**
SnFe	34.04	–	0.5714	4.62	-0.0225	-2.25
SnFeP	33.14	–	0.5399	7.23	-0.0764	-7.64
SnFeP@rGO	33.11	–	0.5260	6.89	-0.1002	-10.02
PdFe/rGO	–	40.13	0.3703	3.21	-0.0483	-4.83
PdFe/SnFeP@rGO	–	40.05	0.3435	2.26	-0.1171	-11.71
Pd/SnFeP@rGO	–	40.10	0.3785	2.84	-0.0272	-2.72
Pd/rGO	–	39.11	0.3983	3.67	+0.0236	+2.36

Ɛ is the lattice constant value of face-centered cubic (fcc) structure of the crystals, D[c] is the average crystallite size obtained from XRD pattern using Scherrer equation ($D = 0.9\lambda / \beta \cos \Theta$), and η[d] is the lattice strain as calculated from Equation: Ƞ = (Ɛ – Ɛ$_o$)/ Ɛ$_o$. Where Ɛ is the lattice constant of Pd alloys in the catalysts, and Ɛ$_o$ is the lattice constant of bulk Pd (0.3891 nm). On the other hand, the Ɛ$_o$ for Sn is 0.5846 nm.

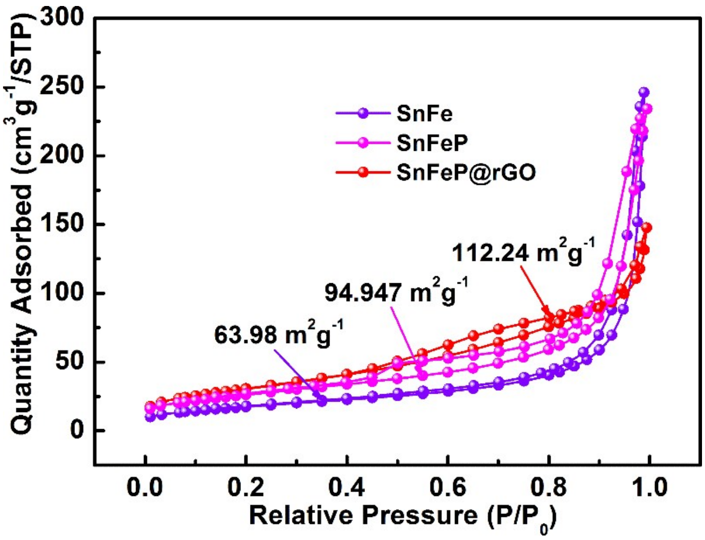

Fig. S2. N_2 adsoption/desorption isotherms of SnFe, SnFeP, and SnFeP@rGO catalysts.

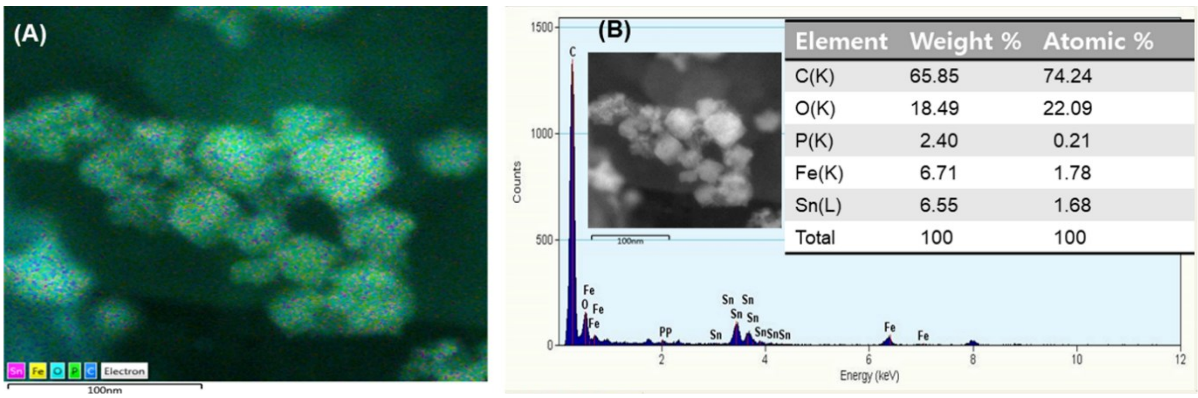

Fig. S3. (A) Elemental mapping, and (B) EDS spectra and composition of SnFeP@rGO.

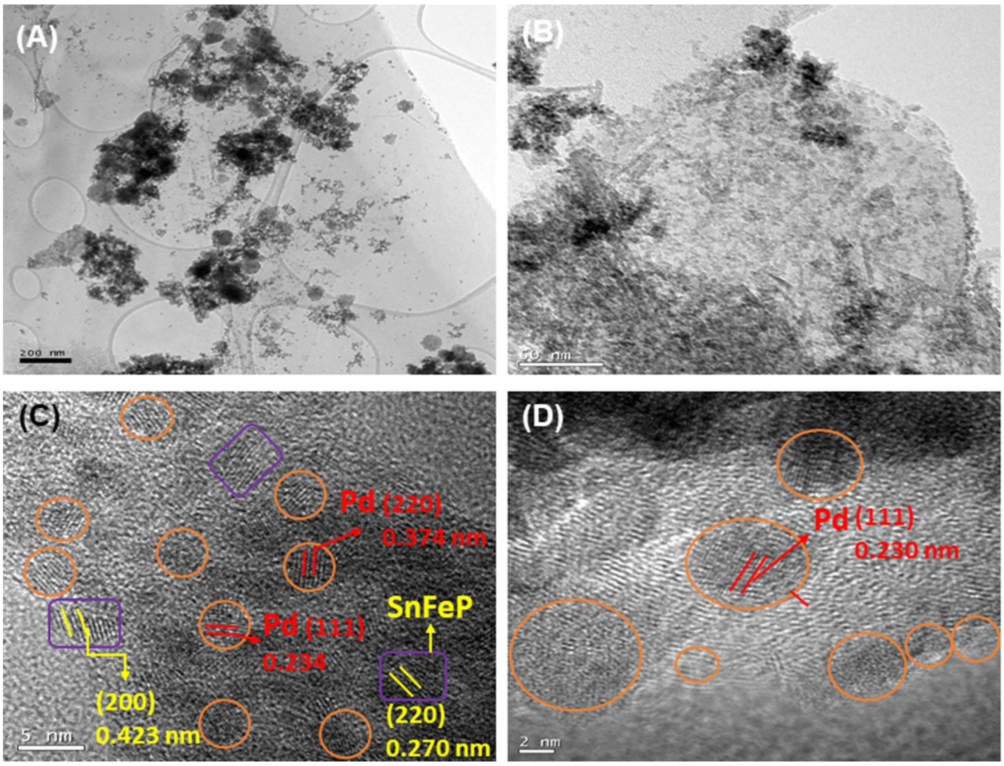

Fig. S4. TEM images of (A) Pd/SnFeP@rGO and (B) Pd/rGO. HR-TEM image of (C) Pd/SnFeP@rGO and (D) Pd/rGO. The scale bar in (B) is 50 nm.

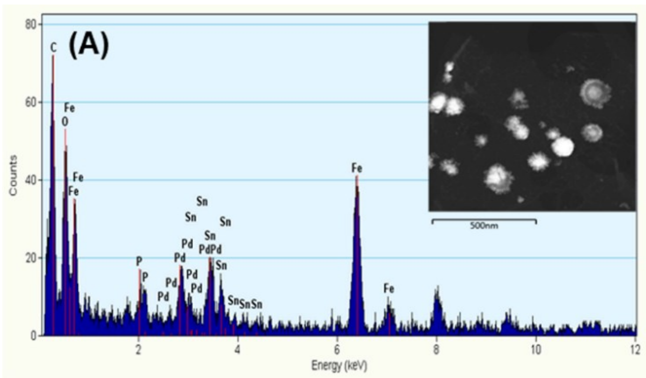

(B)

Element	Weight %	Atomic%
C (K)	53.83	72.51
O(K)	9.42	20.39
P(K)	2.65	0.35
Fe(K)	11.95	5.10
Pd(L)	14.31	0.51
Sn(L)	7.84	1.11
Total	100	100

Fig. S5. (A) EDS data of PdFe/SnFeP@rGO anode catalysts.

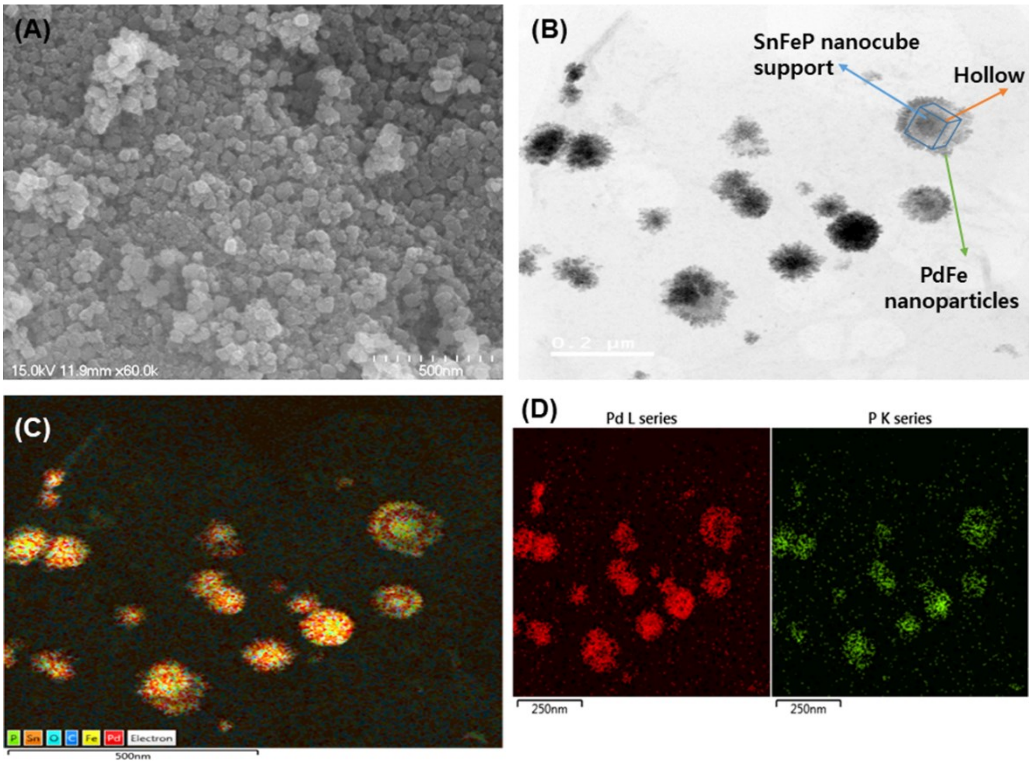

Fig. S6. (A) SEM, (B) TEM image, and (C,D) HAADF-STEM elemental mapping of PdFe/SnFeP@rGO catalyst (repetition of catalyst preparation). (Using SEM, Hitachi S-4200, Japan).

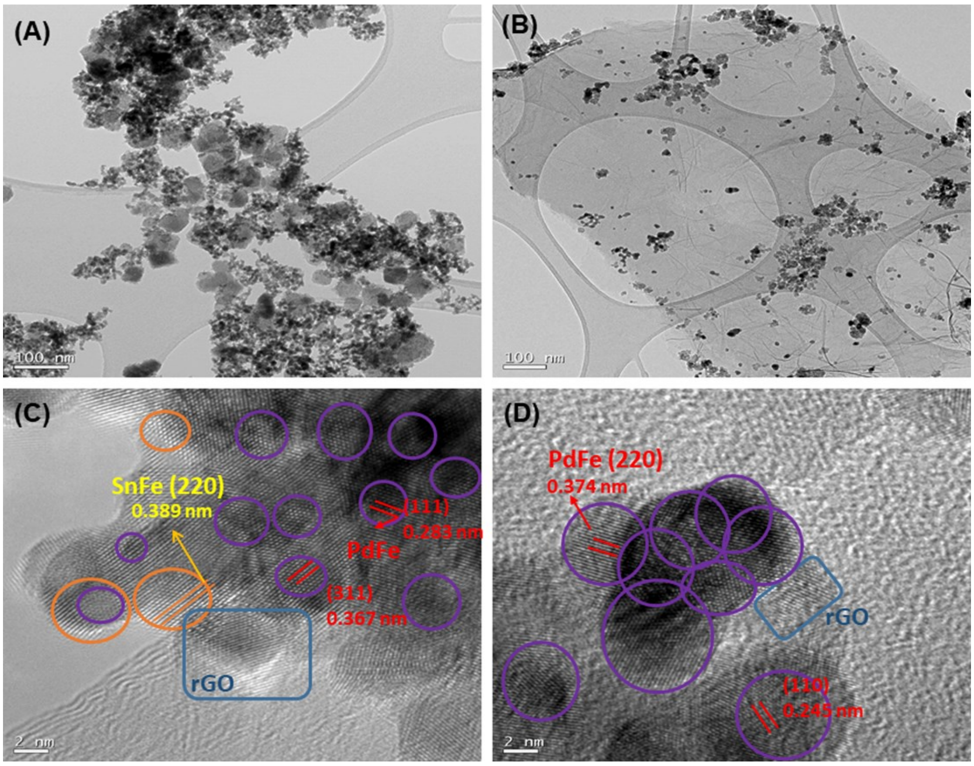

Fig. S7. TEM images of (A,C) PdFe/SnFe@rGO, and (B, D) PdFe/rGO anode catalysts.

Table ST2. Binding energies of Pd based catalysts under XPS investigation.

Catalyst	**Binding Energy (eV)**			
	$Pd3d_{5/2}$		**$Pd3d_{3/2}$**	
	Pd^0	**Pd^{2+}**	**Pd^0**	**Pd^{2+}**
PdFe/SnFeP@rGO	334.90	336.50	340.19	341.71
PdFe/rGO	334.52	336.12	339.81	341.33
Pd/C	334.35	335.95	339.64	341.16

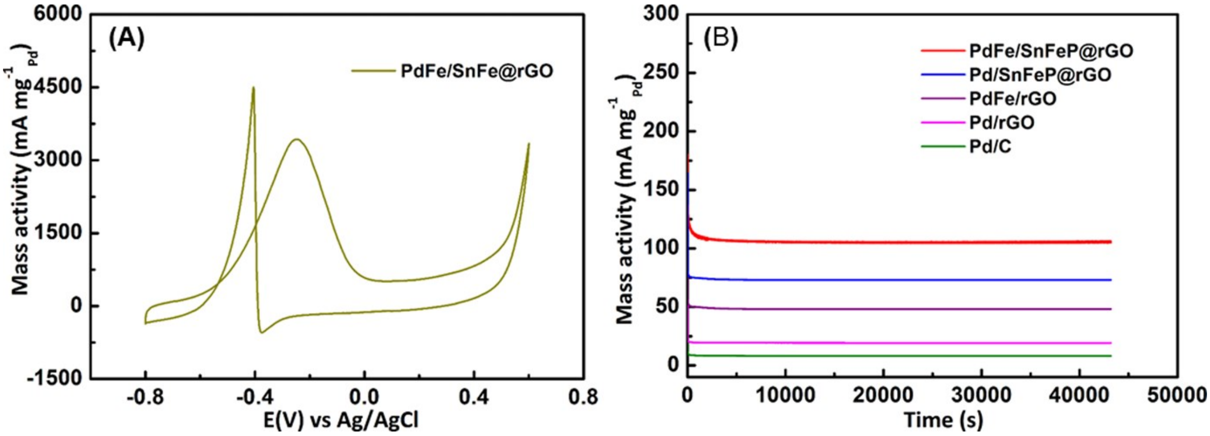

Fig. S8. (A) Mass activity of PdFe/SnFe@rGO catalyst in 0.5 M KOH and 0.3 M ethanol aqueous solution. Scan rate of 10 mVs^{-1}. (B) Chronoamperometric data recorded at 0.1 V *vs.* Ag/AgCl in 0.5 M KOH solution for 12 h.

Table ST3. Summary of catalytic activity with different as-synthesized anode catalysts.

Catalysts	E_{onset} (V *vs.* Ag/AgCl)	ECSA (m^2 g^{-1})	Mass activity (mA mg^{-1}_{Pd})	Specific activity (mA cm^{-2})
PdFe/SnFe@rGO	-0.51	60.05	3431.08	5.71
PdFe/SnFeP@rGO	-0.57	88.65	7135.79	8.04
Pd/SnFeP@rGO	-0.52	68.32	4228.40	6.18
PdFe/rGO	-0.51	59.74	2746.56	4.59
Pd/rGO	-0.48	42.89	945.21	2.20
Pd/C	-0.42	31.47	413.16	1.31

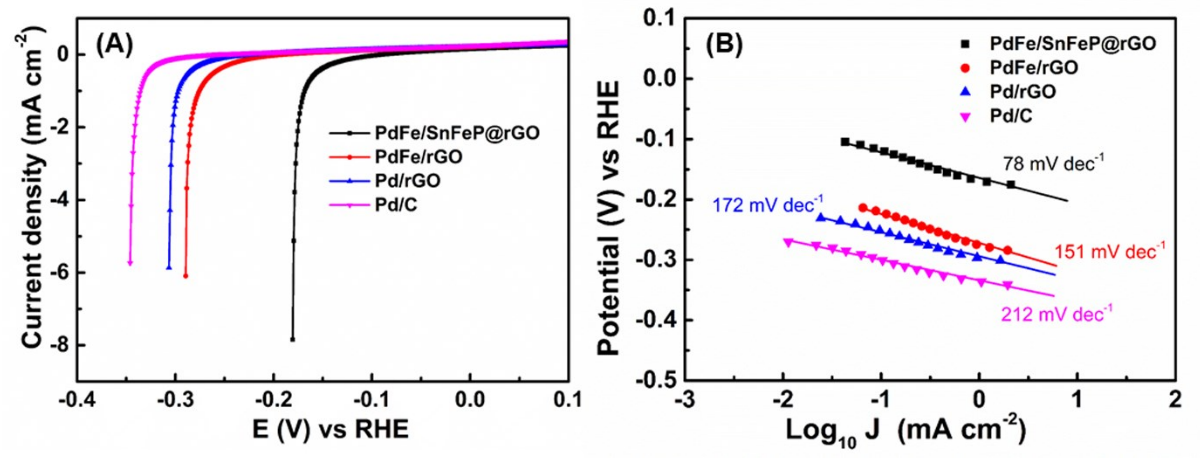

Fig. S9. (A) LSV and, (B) Tafel plot of PdFe/SnFeP@rGO, PdFe/rGO, Pd/rGO, and Pd/C catalyst in 0.5 M KOH. The LSV data were measured at rotating rate 1600 rpm at 2 mV s^{-1} for the electrode at 25 °C. The electrochemical test was performed by continuous passing of N_2 in the alkaline media.

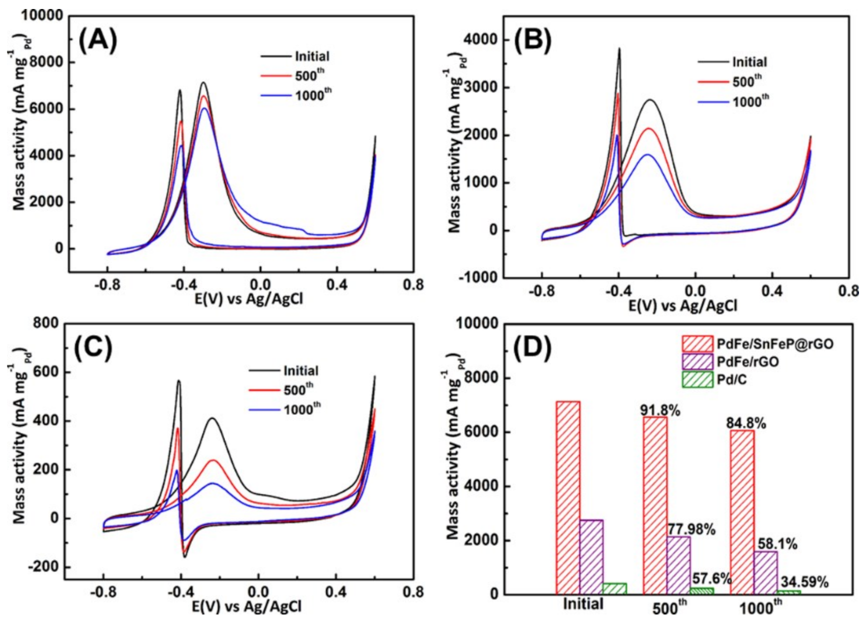

Fig. S10. EOR long-term cycling tests: CV peaks for (A) PdFe/SnFeP@rGO, (B) PdFe/rGO, (C) Pd/C, (D) Percentage of the oxidation peaks current of the 1000 cycles compared to initial cycles using a scan rate of 10 mVs^{-1} in 0.5 M KOH and 0.3 M ethanol aqueous solution.

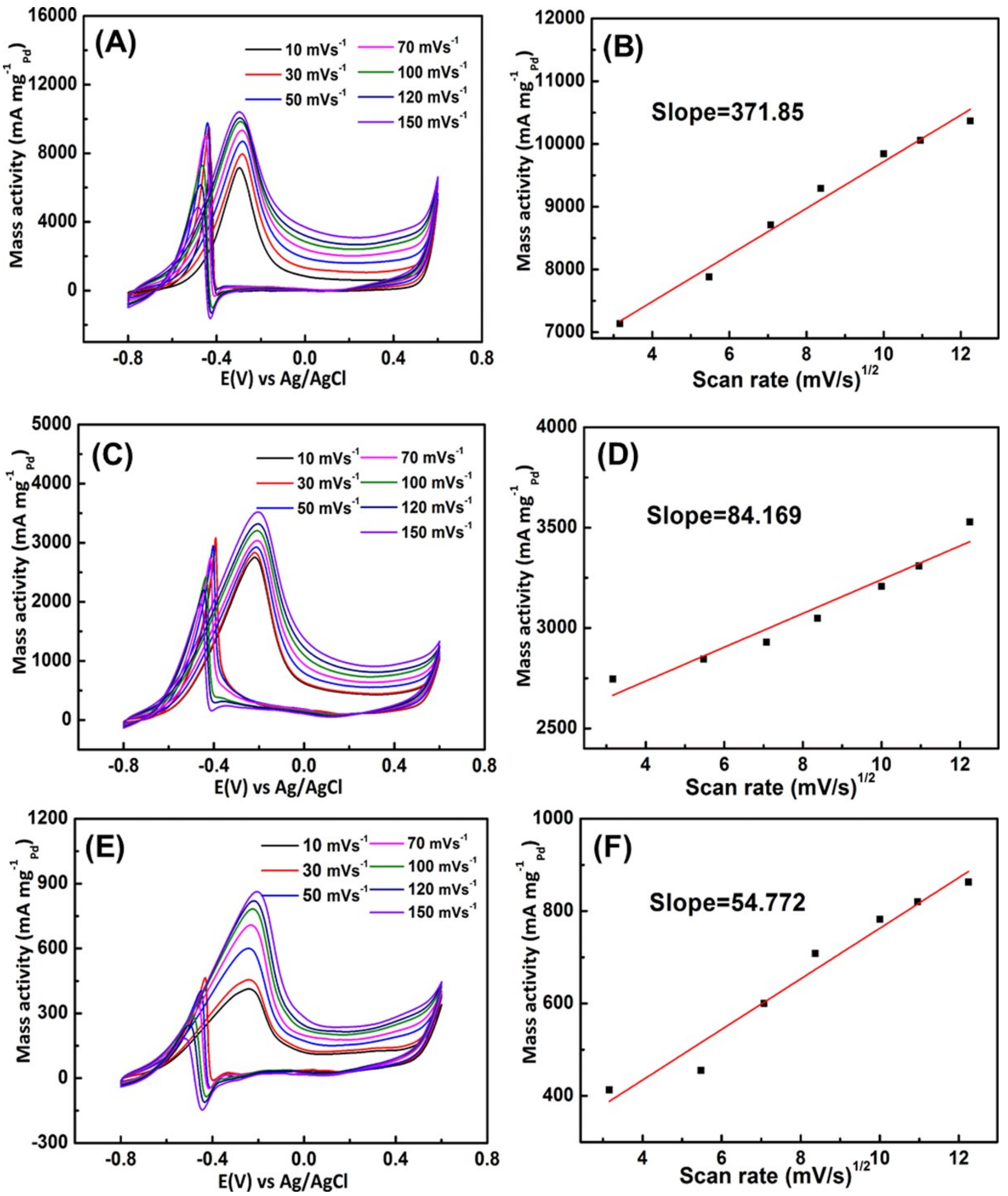

Fig. S11. CV peaks of (A) PdFe/SnFeP@rGO, (C) PdFe/rGO, and (E) Pd/C anode catalysts in 0.5 M KOH and 0.3 M ethanol with different scan rates. (B, D and F) curves of the mass activity vs. square roots of the various scan rate, respectively.

Table ST4. Comparison of electrochemical performance of Pd-based anode catalysts in alkaline medium.

Catalysts	**Electrolyte**	**Mass activity**	**Ref.**
Ultrathin Pd_2Ag_1 NWs	1.0 M KOH + 1.0 M Ethanol	2.84 A mg_{Pd}^{-1}	[1]
Pd-Ni-P	1.0 M NaOH + 1.0 M Ethanol	4.95 A mg_{Pd}^{-1}	[2]
PdP_2/rGO	0.5 M KOH + 0.5 M Ethanol	1.60 A mg_{Pd}^{-1}	[3]
CoP/RGO-Pd10	1.0 M KOH + 1.0 M Ethanol	4.597A mg_{Pd}^{-1}	[4]
Pd_2Sn:P/C	0.5 M KOH + 0.5 M Ethanol	5.02 A mg_{Pd}^{-1}	[5]
Pd/AG-BP	1.0 M NaOH + 1.0 M Ethanol	6.000 A mg_{Pd}^{-1}	[6]
Pd_3NiP/N-rGO	1.0 M KOH + 1.0 M Ethanol	2.223 A mg_{Pd}^{-1}	[7]
c-Pd-Ni-P@a-Pd-Ni-P	1.0 M KOH + 1.0 M Ethanol	3.05 A mg_{Pd}^{-1}	[8]
Pd-P/3DNGS	1.0 M KOH + 1.0 M Ethanol	1.8 A mg_{Pd}^{-1}	[9]
Pd@5%NP/VC	0.5 M KOH + 0.5 M Ethanol	0.777 A mg_{Pd}^{-1}	[10]
PdFe/SnFeP@rGO	0.5 M KOH + 0.3 M Ethanol	7.135 A mg_{Pd}^{-1}	This study

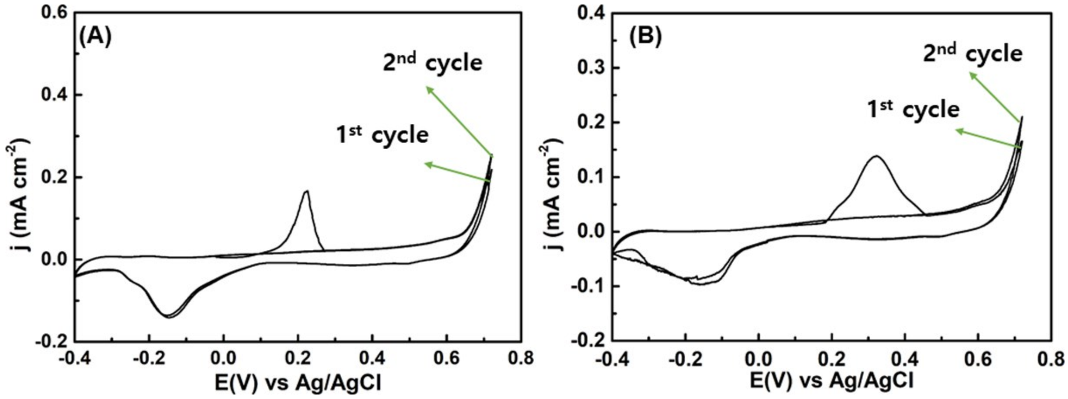

Fig. S12. CO stripping of (A) PdFe/SnFeP@rGO and (B) Pd/C in 0.1 M KOH. Potential scan rate of 10 mV S^{-1} at 25 °C.

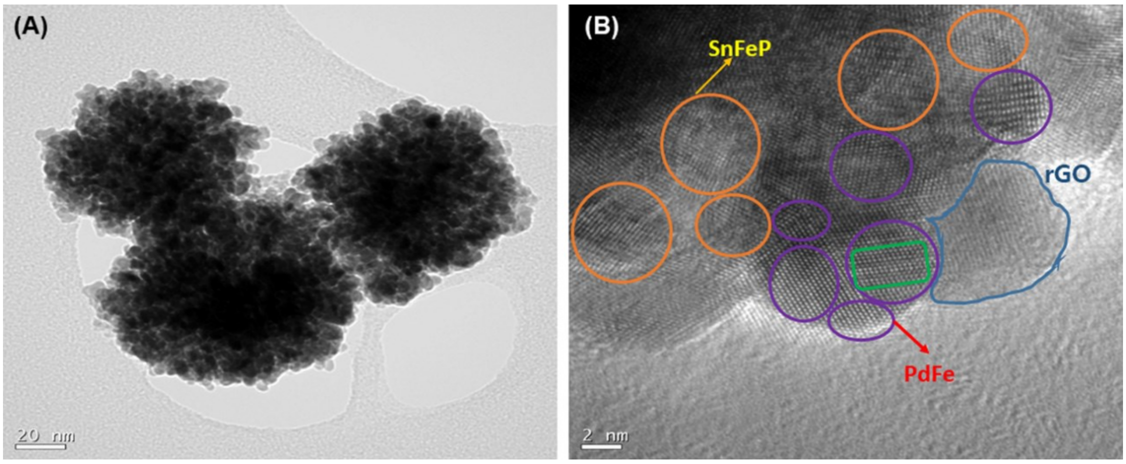

Fig. S13. TEM and HR-TEM of PdFe/SnFe@rGO catalyst after CO stripping test.

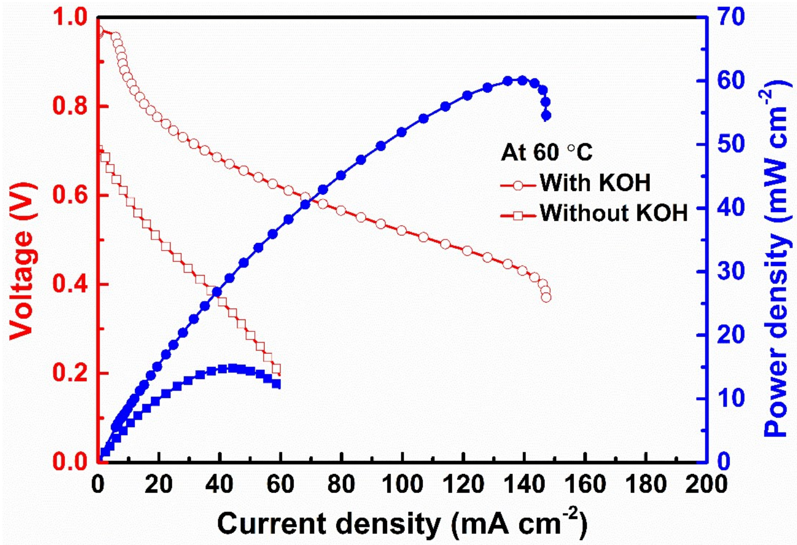

Fig. S14. Polarization curve of PdFe/SnFeP@rGO with and without 0.5 M KOH and 1.0 M ethanol at 60 °C.

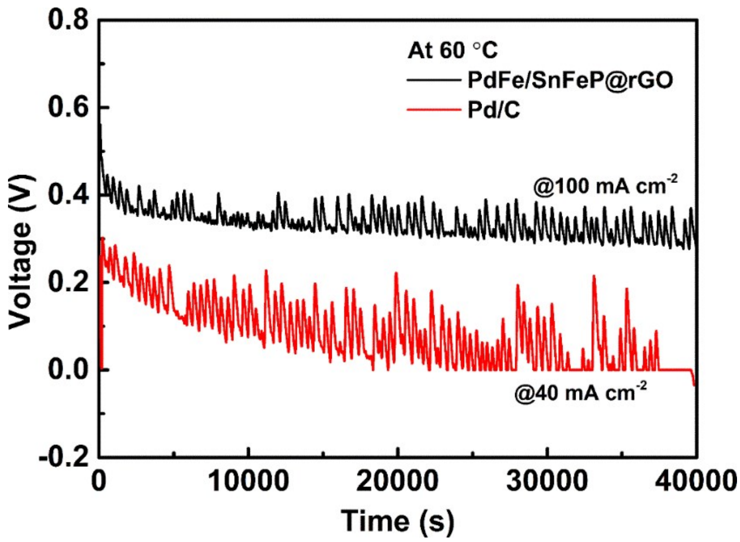

Fig. S15. Stability test of a PdFe/SnFeP@rGO cell at a constant load current density of 100 mA cm^{-2} at 60 °C and Pd/C cell at a constant load current density of 40 mA cm^{-2} at 60 °C with 0.5 M KOH and 1.0 M ethanol solution as fuel.

Table ST5. DEFCs performance with Pd based catalysts.

Anode catalysts	Cathode catalysts	Membrane	T °C	Fuel	MPD (mW cm^{-2})	Ref.
In_3Pd_2	Pt/C	Nafion 115	70	1 M ethanol + 1 M KOH	6.7	[11]
$Pd_{89.3}Au_{10.7}$	Pt/C	AEM (A201)	40	1 M ethanol + 1 M KOH	31.5	[12]
Pd_1Sn_3/Vulcan XC-72	Pt/C	Nafion 117	80	2 M ethanol + 1 M KOH	42	[13]
Pd_2Ru/C	MnO_2 nano-rod	Tokuyama A201	60	2 M ethanol + 1 M KOH	38.9	[14]
Pd_1Nb_1/C	Pt/C	Nafion 117	70	2 M ethanol + 1 M KOH	27	[15]
$Pt_{36}Pd_{41}Cu_{23}$ NWs	Pt/C	Nafion 115	80	2 M ethanol	21.7	[16]
PdSn(50:50)/C	Pt/C	Nafion 117	60	1 M ethanol + 1 M KOH	20	[17]
Pd_7IrNi_{12}/C	Fe-Co HTM K14	Tokuyama A201	60	1 M ethanol +1 M KOH	49	[18]
PdFe/SnFeP@rGO	Pt/C	Nafion 117	60	1 M ethanol + 0.5 M KOH	60.24	This study

*MPD = Maximum power density, T = Temperature, Ref = Reference,

DEFCs = Direct ethanol fuel cells.

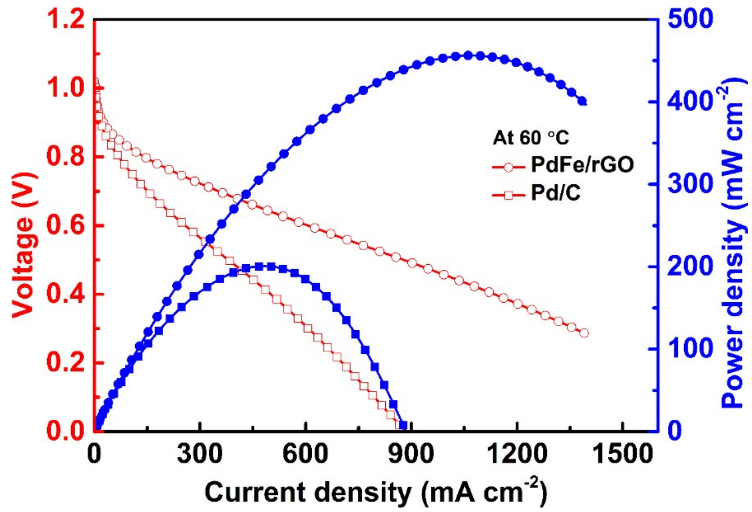

Fig. S16. Polarization curves of PdFe/rGO (30% Pd) and commercial Pd/C (40% Pd) in hydrogen gas at 60 °C.

Table ST6. Single cell performance of Pd based catalysts in hydrogen fuel.

Anode catalysts	Cathode catalysts	Membrane	T °C	Fuel/ Oxidant	MPD (mW cm^{-2})	Ref
Pd_3Co/PCNT	Pt/C	Nafion 212	60	H_2/O_2	327	[19]
$Pd_{0.33}Ir_{0.67}$/N-C	Pt/C	QASEBS	79	H_2/O_2	514	[20]
Pd/C-CeO_2 (20 wt% Pd)	Pt/C	AEM	73	H_2/air	460	[21]
Pd-Co/gCN	Pt/C	Nafion 212	60	H_2/O_2	290	[22]
Pd/C-CeO_2	Pt/C	AEM	73	H_2/air	500	[23]
Pd/Ni	Ag alloy	AEM	73	H_2/air	400	[24]
PdFe/SnFeP @rGO	Pt/C	Nafion 117	60	H_2/O_2	857.54	This study

*MPD = Maximum power density, T = Temperature, Ref = Reference

References

[1] H. Lv, Y. Wang, A. Lopes, D. Xu and B. Liu, Ultrathin PdAg single-crystalline nanowires enhance ethanol oxidation electrocatalysis. *Appl. Catal. B: Environ.*, 2019, **249**, 116–125. doi.org/10.1016/j.apcatb.2019.02.068.

[2] L. Chen, L. Lu, H. Zhu, Y. Chen, Y. Huang, Y. Li and L. Wang, Improved ethanol electrooxidation performance by shortening Pd–Ni active site distance in Pd–Ni–P nanocatalysts. *Nat. Commun.,* 2017, **8**,14136. doi.org/10.1038/ncomms14136.

[3] J. Liu, Z. Luo, J. Li, X. Yu, J. Liorca, D. Nasiou, J. Arbiol, M. Meyns and A. Cabot, Graphene-supported palladium phosphide PdP_2 nanocrystals for ethanol electrooxidation. *Appl. Catal. B: Environ.,* 2019, **242**, 258–266. doi.org/10.1016/j.apcatb.2018.09.105.

[4] M. Wang, R. Ding, Y. Xiao, H. Wang, L. Wang, C. M. Chen, Y. Mu, G. P. Wu and B. Lv, CoP/RGO-Pd hybrids with heterointerfaces as highly active catalysts for ethanol electrooxidation. *ACS Appl. Mater. Interfaces,* 2020, **12**, 28903–28914. doi.org/10.1021/acsami.0c07703

[5] X. Yu, J. Liu, J. Li, Z. Luo, Y. Zuo, C. Xing, J. Llorca, D. Nasiou, J. Arbiol, K. Pan, T. Kleinhanns and Y. Xie, A. Cabot. Phosphorous incorporation in Pd_2Sn alloys for electrocatalytic ethanol oxidation. *Nano Energy,* 2020, **77**, 105116. doi.org/10.1016/j.nanoen.2020.105116.

[6] T. Wu, Y. Ma, Z. Qu, J. Fan, Q. Li, P. Shi, Q. Xu and Y. Min, Black phosphorus–graphene heterostructure-supported Pd nanoparticles with superior activity and stability for ethanol electro-oxidation. *ACS Appl. Mater. Interfaces*, 2019, **11**, 5136–5145. doi.org/10.1021/acsami.8b20240.

[7] S. R. Chowdhury, T. Maiyalgan, S. K. Bhattachraya and A. Gayen, Influence of phosphorus on the electrocatalytic activity of palladium nickel nanoalloy supported on N-doped reduced graphene oxide for ethanol oxidation reaction. *Electrochim. Acta,* 2020, **342**, 136028. doi.org/10.1016/j.electacta.2020.136028.

[8] P. F. Yin, M. Zhou, J. Chen, C. Tan, G. Liu, Q. Ma, Q. Yun, X. Zhang, H. Cheng, Q. Lu, B. Chen, Y. Chen, Z. Zhang, J. Huang, D. Hu, J. Wang, Q. Liu, Z. Luo, Z. Liu, Y. Ge, X. J. Wu, X. W. Du and H. Zhang, Synthesis of palladium-based crystalline@amorphous core–shell nanoplates for highly efficient ethanol oxidation. *Adv. Mater.*, 2020, **32**, 2000482. doi.org/10.1002/adma.202000482.

[9] H. Yang, S. Li, R. Jin, Z. Yu, G. Yang and J. Ma, Surface engineering of phosphorus low-doping palladium nanoalloys anchored on the three-dimensional nitrogen-doped graphene for enhancing ethanol electroxidation. *Chem. Eng. J,* 2020, **389**, 124487. doi.org/10.1016/j.cej.2020.124487.

[10] R. Kottayintavida and N. K. Gopalan, Nickel phosphate modified carbon supported Pd catalyst for enhanced alcohol electro oxidation. *Int. J. Hydrogen Energy,* 2020, **45**, 11116–11126. doi.org/10.1016/j.ijhydene.2020.02.050.

[11] Y. J. Chen, Y. R. Chen, C. H. Chiang, K. L. Tung, T. K. Yeh and H. Y. Tuan, Monodisperse ordered indium-palladium nanoparticles: synthesis and role of indium for boosting superior electrocatalytic activity for ethanol oxidation reaction. *Nanoscale,* 2019, **11**, 3336–3343. doi:10.1039/C8NR07342B.

[12] A. S. Douk, H. Saravani, M. Z. Y. Abad and M. Noroozifar, Three-Dimensional engineering of nanoparticles to fabricate a Pd-Au aerogel as an advanced supportless electrocatalyst for low-temperature direct ethanol fuel cells. *ACS Appl. Energy Mater.*, 2020, **3**, 7527–7534. doi.org/10.1021/acsaem.0c00928.

[13] V. S. Pinheiro, F. M. Souza, T. C. Gentil, A. N. Nascimento, P. Bohnstedt, L. S. Parreira, E. C. Paz, P. Hammer, M. I. Sairre, B. L. Batista and M. C. Santos, Sn-containing electrocatalysts with a reduced amount of palladium for alkaline direct ethanol fuel cell applications. *Renew. Energy,* 2020, **158**, 49–63. doi.org/10.1016/j.renene.2020.05.050.

[14] J. Gua, R. Chen, F. C. Zhu, S. G. Sun and H. M. Villullas, New understandings of ethanol oxidation reaction mechanism on Pd/C and Pd_2Ru/C catalysts in alkaline direct ethanol fuel cells. *Appl. Catal. B: Environ.*, 2018, **224**, 602–611. doi.org/10.1016/j.apcatb.2017.10.037.

[15] F. M. Souza, P. Bohnstedt, V. S. Pinheiro, L. A. Oliveira, B. L. Batista, L. S. Parreira and R. A. Antunes, M. C. Santos, Niobium increasing the electrocatalytic activity of palladium for alkaline direct ethanol fuel cell. *J. Electroanal. Chem.,* 2020, **858**, 113824. doi.org/10.1016/j.jelechem.2020.113824.

[16] K. Wang, F. Wang, Y. Zhao and W. Zhang, Surface-tailored PtPdCu ultrathin nanowires as advanced electrocatalysts for ethanol oxidation and oxygen reduction reaction in direct ethanol fuel cell. *J. Energy Chem.*, 2021, **52**, 251–261 (2021). doi.org/10.1016/j.jechem.2020.04.056.

[17] E. H. Fontes, C. E. D. Ramos, J. Nandenha, R. M. Piasentin, A. O. Neto and R. Landers, Structural analysis of PdRh/C and PdSn/C and its use as electrocatalysts for ethanol oxidation in alkaline medium. *Int. J. Hydrogen Energy,* 2019, **44**, 937–951. doi.org/10.1016/j.ijhydene.2018.11.049.

[18] S. Shen, T. S. Zhao, J. Xu and Y. Li, High performance of a carbon supported ternary PdIrNi catalyst for ethanol electrooxidation in anion exchange membrane direct ethanol fuel cells. *Energy Environ. Sci.*, 2011, **4**, 1428–1433. doi: 10.1039/C0EE00579G.

[19] P. Chandran and S. Ramaprabhu, Catalytic performance of non-platinum-based hybride carbon hetero-structure for oxygen reduction and hydrogen oxidation reactions in proton exchange membrane fuel cell. *Int. J. Hydrogen Energy,* 2018, **43**, 18477–18487. doi.org/10.1016/j.ijhydene.2018.08.066.

[20] Y. Cong, I. T. McCrum, X. Gao, Y. Lv, S. Miao, Z. Shao, B. Yi, H. Yu, M. J. Janik and Y. Song, Uniform $Pd_{0.33}Ir_{0.67}$ nanoparticles supported on nitrogen –doped carbon with remarkable activity toward the alkaline hydrogen oxidation reaction. *J. Mater. Chem. A,* 2019, **7**, 3161–3169. doi:10.1039/C8TA11019K.

[21] H. A. Miller, F. Vizza, M. Marelli, A. Zadick, L. Dubau, M. Chatenet, S. Geiger, S. Cherevko, H. Doan, R. K. Pavlicek, S. Mukerjee and D. R. Dekel, Highly active nanostructured palladium-ceria electrocatalysts for the

hydrogen oxidation reaction in alkaline medium. *Nano Energy,* 2017, **33**, 293–305. doi.org/10.1016/j.nanoen.2017.01.051.

[22] A. Ghosh, P. Chandran and S. Ramaprabhu, Palladium-nitrogen coordinated cobalt alloy towards hydrogen oxidation and oxygen reduction reactions with high catalytic activity in renewable energy generations of proton exchange membrane fuel cell. *Appl. Energy*, 2017, **208**, 37–48. doi.org/10.1016/j.apenergy.2017.10.022.

[23] H. A. Miller, A. Lavacchi, F. Vizza, M. Marelli, F. D. Benedetto, F. D. Acapito, Y. Paska, M. Page and D. R. Dekel, Pd/C-CeO2 Anode Catalyst for High-Performance Platinum-Free Anion Exchange Membrane Fuel Cells. *Angew. Chem. Int. Ed.*, 2016, **55**, 6004–6007. doi.org/10.1002/anie.201600647.

[24] M. Alesker, M. Page, M. Shviro, Y. Paska, G. Gershinsky, D. R. Dekel and D. Zitoun, Palladium/nickel bifunctional electrocatalyst for hydrogen oxidation reaction in alkaline membrane fuel cell. *J. Power Sources*, 2016, **304**, 332–339. doi.org/10.1016/j.jpowsour.2015.11.026.